Comparison of anomalies in the VLF spectrum of the natural electromagnetic field with data from the seismometer in a landslide-affected area

Michal HOFFMAN[1,2,*] 🆔, Eduard KOČI[1,2] 🆔

[1] Earth Science Institute, Slovak Academy of Sciences,
   P.O. Box 106, Dúbravská cesta 9, SK-840 05, Bratislava, Slovak Republic

[2] Comenius University in Bratislava, Faculty of Science, Department of Engineering Geology,
   Hydrogeology and Applied Geophysics,
   Mlynská dolina, Ilkovičova 6, 842 15 Bratislava, Slovak Republic

Abstract: The data from a permanent monitoring station, based on a sound card as an AD/DA converter and a magnetic loop antenna for continuous recording of electromagnetic field intensities in the Very Low Frequency (VLF) range, were recorded and compared with data from a seismic station based on Raspberry Pi located in a landslide-affected area. The stations operated 24/7 and were placed in a room below ground level. Correlations were observed between seismic signals in the frequency spectrum from 0.1 Hz to 10 Hz (some extending beyond 20 Hz) and anomalies in the electromagnetic field in the VLF range. These anomalies are likely associated with micro-fracturing, piezo-electromagnetic, and triboelectric phenomena within the landslide body, producing relatively weak VLF emissions and a faint seismic signal. A single-component 4.5 Hz 395 Ohm vertical Racotech RGI-20DX geophone with electronic extension to lower frequencies (<1 Hz) was used with a sampling rate of 100 sps (samples per second). VLF emissions cover almost the entire spectrum from 6 kHz with a peak at 14 kHz to 18 kHz. The received spectrum was divided into following sections: VLF band 4 kHz – 6 kHz; 6 kHz – 8 kHz; 8 kHz – 10 kHz; 10 kHz – 12 kHz; 12 kHz – 14 kHz; 14 kHz – 16 kHz; 16 kHz – 18 kHz. Simultaneously, there were changes in these sections analysed and compared with the seismic record within the same time interval.

Key words: landslides, very low frequency, seismometer, natural radio emissions

1. Introduction

Several authors from various scientific fields, including geology, geophysics, and electrical engineering, have explored the issue of electromagnetic emissions on slopes affected by landslides (*Mastow et al., 1989a; Mastow et al.,*

---

*corresponding author, e-mail: hoffman2@uniba.sk

1989b; Kharkhalis, 1995; Vybíral, 2002; Blaha and Duras, 2004; Fabo et al., 2004; Jaroševič and Kundracík, 2004; Koktavý and Šikula, 2004; Maniak, 2015; Maniak and Mydlikowski, 2023). The generation of electromagnetic emissions in the geological environment had been studied for decades by both domestic and foreign scientists from various geoscience areas *(Hanson and Rowell, 1980; Gershenzon and Bambakidis, 2001; Koktavý and Šikula, 2004; Rabinovitch et al., 2000; Takeuchi and Nagahama, 2006; Hayakawa, 2015).* Laboratory experiments and field observations had revealed that electromagnetic emissions are primarily generated in rocks and the geological environment through piezo-electromagnetic phenomena, triboelectricity *(Adler, 2001; Eccles et al., 2005; Heister et al., 2005),* and streaming potential of electrolyte flowing through pores in rocks *(Reppert et al., 2001).* EM emissions also had occurred during the propagation of fractures where crack walls create an electric charge that varies over time during the propagation of the crack *(Krumbholz, 2010).* Slope movements in the area could manifest as slides, slumps, surface creeping, and soil collapses *(Otepka et al., 1983).* Additionally, debris flows, extensional erosional grooves (formed by a combination of rainfall erosion and the removal of fine material along with extension caused by the "flowing" of the slope with a motion vector parallel to the length of the erosional groove), and classic rotational-translational landslides could be observed in the field. The activity of landslides in the studied area is influenced by climate changes and the erosive activity of the Váh River. The goal of the study is to compare the seismic response of movement on the landslide mass *(Arattano et al., 1999; Amitrano et al., 2007; Tonnellier et al., 2013; Fiorucci et al., 2022)* with in-situ VLF anomalies.

2. Material and methods

2.1. Settings and technologies

VLF acquisition:

There were recorded 24/7 time series of the seismic component along with the time series of VLF electromagnetic field intensity using a combined geophysical station. These have provided continuous measurement of the electromagnetic field in the Very Low Frequency (VLF) range (Figs. 1, 2) and continuous measurement using a seismometer *(Arattano et al., 1999; Amitrano et al., 2007; Tonnellier et al., 2013; Fiorucci et al., 2022).*
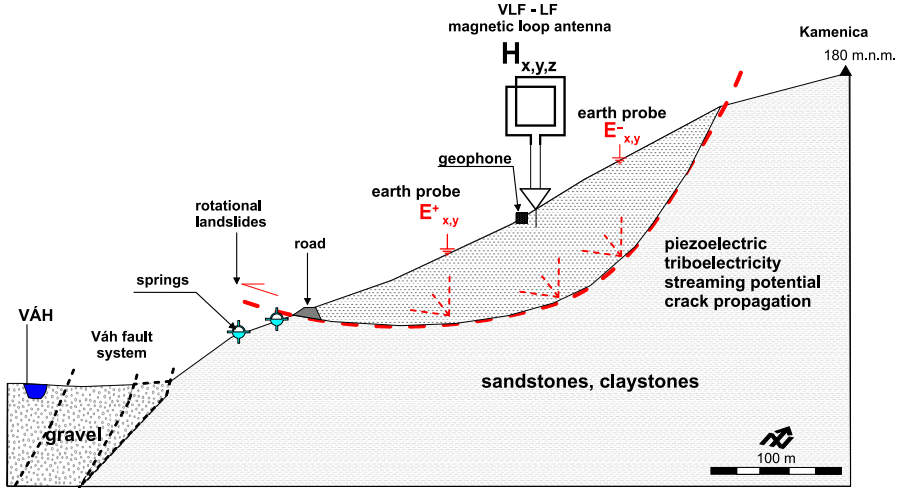
Fig. 1. The position of the VLF EasyLoop antenna, VLF earth probes, and seismometer in the field. The loop antenna is highly directional and is oriented parallel to the slope, N–S.

Our station is located in an area of active slope movements on the western edge of the Nitrianská "Zálužianska" hills near the village of Vinohrady nad Váhom in the Galanta district (Slovakia). There is a sound card labeled ADA-71 USB with a CMedia CM6206 chipset and a sampling frequency of 48 kHz or Behringer UMC HD204 with 192 kHz sampling rate used to re-
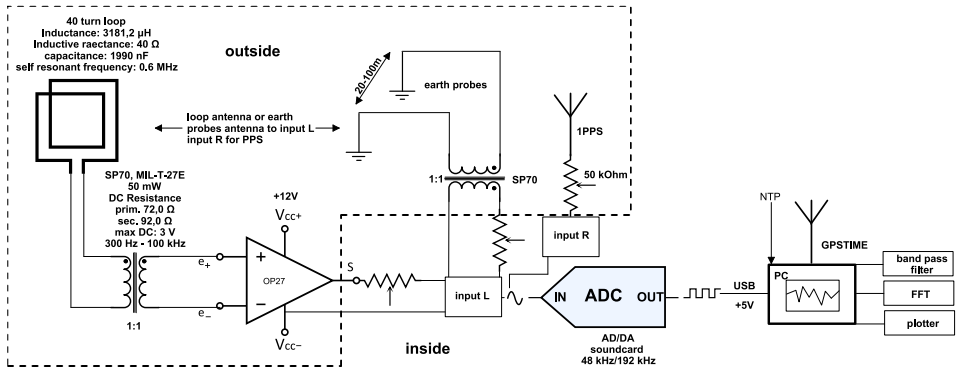

Fig. 2. Description of the antenna system components (loop H-field antenna and earth probes) and ADC converter along with the injection of the 1PPS signal NTP and GPS-TIME.

ceive Very Low-Frequency waves. An amplifier based on OP27 for the Very Low-Frequency range is connected to the input of the sound card, installed directly on the magnetic loop antenna (Fig. 1) with NNE–SSW orientation approximately parallel to the base of the hills and with minimal noise in that direction (Fig. 2). When it comes to receiving the magnetic and electric components, only one is received if PPS is used because it goes into the second input of the sound card. If PPS is not used (we calibrate using, for example, DCF77 or DHO23), it is possible to record both components as the Left channel for, e.g., magnetic, and the Right channel for the electric component. They are recorded separately into one file, which is then split into the right and left channels and analysed separately. Before entering the sound card, a transformer is used in both cases, specifically the SP70 model. If a PPS signal is introduced for calibration, the transformer is not used, but a 50 kOhm potentiometer is used instead because the PPS signal from GPS is too strong and needs to be attenuated (Fig. 2).

Geological and tectonic setting of landslides belt "Hlohovec – Sereď" based on field work and field observation is described in work *Hoffman (2022)*.

A recording VLF station and a seismometer are continuous monitoring stations that record VLF electromagnetic fields within specified frequency ranges and ground tremors in the landslide area. VLF and seismic the station uses GPS and/or NTP timing (*sudo systemctl start ntp* in terminal) and we use the DHO38 station for oscillator correction. The second permanent VLF station located about 4 km south uses GPS timing and uses the DCF77 signal and/or the 1PPS signal from GPS to correct the oscillations of the oscillator. This receiving system, as implied by the antenna type, captures the magnetic component of the electromagnetic field in the Very Low-Frequency range. The sound card is connected to a laptop running on UBUNTU OS v.22 (Linux), where the SpectrumLab recording software (*Buescher, 2020*) is running (Fig. 3). The exact description of recording methodology of the electromagnetic field in the VLF band is provided in the previous article (*Hoffman, 2023*). The visualization, saving, and analysis of received electromagnetic spectrum is provided with this software. The received spectrum is divided into following sections: VLF band 4 kHz – 6 kHz; 6 kHz – 8 kHz; 8 kHz – 10 kHz; 10 kHz – 12 kHz; 12 kHz – 14 kHz; 14 kHz – 16 kHz; 16 kHz – 18 kHz, 18 kHz – 23 kHz and as a whole, 4 kHz –

18 kHz (if necessary), each section graphically visualized as a line graph of VLF EM field intensity (dB) over time (Fig. 3).
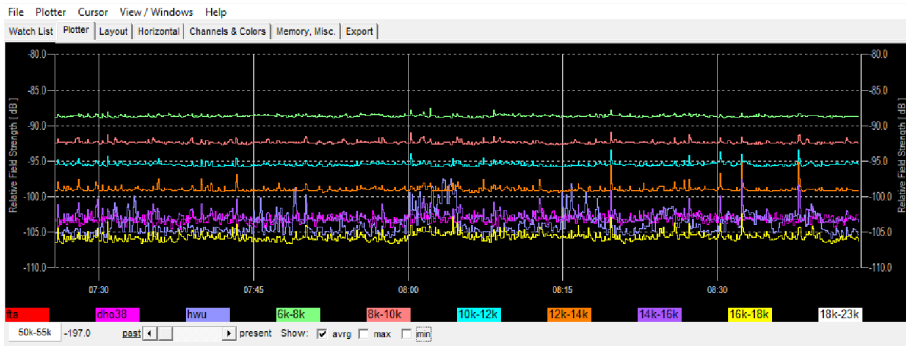

Fig. 3. Example graphic record from permanent VLF station of intensities over time in the divided electromagnetic field (magnetic component) in 2 kHz-wide sections using SpectrumLab software. Dated February 24th, 2023, spanning from 07:25 to 08:45 UTC.

Frequencies below 4 kHz are not being analysed due to the intensity of artificial noise in this range. The width of the received radio band depends on the sampling frequency of the sound card (AD/DA converter). In our case, the sampling frequency is 48 kHz or 192 kHz, allowing us to monitor the VLF band from DC to 24 kHz or up to 91.5 kHz.

Seismic acquisition:

The VLF recording system is complemented by a seismometer based on Raspberry Pi v.4 (Fig. 4). This plug-and-play seismometer is equipped with infrasound recording (a comparison of VLF field and infrasound changes will be published later). The operating system of the seismometer control unit is Debian 8 (Linux). The data format for recording seismic data is miniSEED compatible with various seismic applications such as SeisComP3, Earthworm, Antelope, and others. The data is regularly transmitted to the USGS seismic network via the Swarm program.

Geophone setting:

The geophone itself is a single-component 4.5 Hz 395 Ohm vertical Racotech RGI-20DX geophone with electronic extension to lower frequencies (< 1 Hz) with a sampling rate of 100 sps. The frequency range of the geophone is −3 dB points at 0.7 and 44 Hz. The applied filters are: −1 (0.16 Hz, single-

pole high-pass filter), -3.03×2 (0.48 Hz, double-pole high-pass filter), -666.67 (106 Hz, single-pole low-pass filter). The sensitivity of the geophone is 3.996500E+08 counts/meter/second $+/-$ 10% precision. Timing is ensured using the NTP protocol, with timing quality remaining within 1 sample of accuracy versus startup accuracy: $+/-$ 10 ms or better for 100 sps (*Raspberry manual*, `https://manual.raspberryshake.org/`). Data connectivity is provided by a 4G modem. Daily records are downloaded from both devices over an 8-hour time span, primarily from 22:00 UTC to 06:00 UTC.
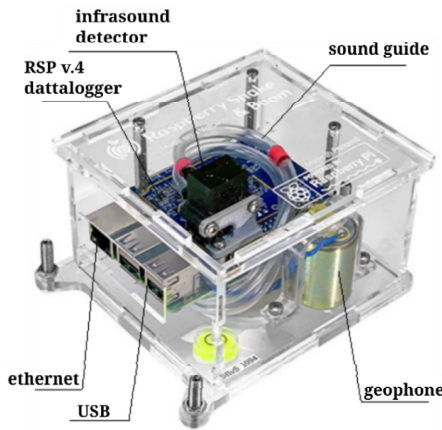

Fig. 4. A seismometer based on Raspberry Pi, combined with the measurement of infrasound, utilizing the Raspberry Shake platform (`https://manual.raspberryshake.org/`).

This time range was chosen to minimize anthropogenic noise during these night-time hours and was adjusted based on the noise intensity in the vicinity. Daily records from other time intervals of the day were archived but have not been analysed yet. Downloaded data from the seismometer during the specified time period are converted from miniSEED format to graphical form using the Swarm program. The time series is plotted with time on the "x" axis and intensity on the "y" axis. Seismic data is filtered using the web interface of the seismometer in the frequency range of $0.1\,\mathrm{Hz}-1\,\mathrm{Hz}$, $0.7\,\mathrm{Hz}-2\,\mathrm{Hz}$, and $3\,\mathrm{Hz}-7\,\mathrm{Hz}$. The filter used is adopted from earlier works on seismic response to landslide masses, mainly from the work of *Amitrano et al. (2007), Yamada et al. (2012), Tonnellier et al. (2013)* and *Lin et al. (2015).*

Subsequently, data from the VLF monitoring station is downloaded for the same time interval as the seismometer. The data from the VLF station is in text format (*.txt), which is converted into a tabular form using MS Excel. Tabular intensity data for each VLF band (8 kHz – 10 kHz; 10 kHz – 12 kHz; 12 kHz – 14 kHz; 14 kHz – 16 kHz; 16 kHz – 18 kHz, and as a whole 4 kHz – 18 kHz or up to 18 kHz – 23 kHz) is graphically represented in an "x, y" graph, similar to the seismic data, showing the dependency on time (axis "x"). Combination of obtained time-graphic records from both channels (seismic and VLF channels) are visually unified with the same time intervals and simultaneously compared of both components. There is necessary to exclude all peaks caused by thunderstorm activity, which significantly influence recording time of the VLF spectrum, mainly in the range from 4 kHz to 15 kHz with a peak at 11 kHz. Data from seismogram to download are available on: `https://data.raspberryshake.org/fdsnws/dataselect/1/builder` (*Raspberry data*).

2.2. Data evaluation methodology

Prepared data were subjected to a mathematical correlation analysis. Pearson correlation coefficient 'r' was used for calculation of the correlation coefficient, using following formula (1) (*Pearson, 1907*):

$$r = \frac{\sum (x_i - \bar{x})(y_i - \bar{y})}{\sqrt{\sum (x_i - \bar{x})^2 \sum (y_i - \bar{y})^2}}, \tag{1}$$

x_i, y_i are the values of the variables "x" (intensity of VLF signals) and "y" (seismic signal), $\bar{x}$, $\bar{y}$ are the means of the variables "x" and "y". This formula can be used to calculate the Pearson correlation coefficient (denoted as r) for two sets of data, "x" and "y". The closer r is to 1, the stronger the positive correlation. The closer r is to -1, the stronger the negative correlation.

If coefficient r is close to 0, it indicates little or no correlation between the variables. The equation (2) was used for calculation of expected radio anomalies frequency, where t_{prop} is the crack propagation time in the rock material with the crack length l_{frac} in the rock block, considering that the crack propagation speed could be close to the speed of seismic P waves.

The length l_{frac} is the characteristic length of cracks observed in the field, created under the given conditions in the given rock environment in the area

73

we investigated (*Hoffman, 2023*), and that is about 1m. In the calculation of the frequency of anomalies, the (seismic) propagation velocities of cracks enter approximately $1100-2500$ m.s^{-1} for clay a $1500-2000$ m.s^{-1} for wet sands (*Schumann et al., 2014*).

$$t_{prop} = \frac{l_{frac}}{v_{seis}} \ [\text{s}] \,. \tag{2}$$

To calculate the rate of crack formation, there was used the inverse value (3) of the calculated crack propagation time (*Martinelli et al., 2020*):

$$f_{anom} = \frac{1}{t_{prop}} \ [\text{Hz}] \,. \tag{3}$$

Generally in the literature, there are various relations (4) for calculating the frequency of the electromagnetic field generated by crack propagation, for instance as the one described by *Martinelli et al. (2020)* as follows:

$$\omega = \frac{v_{el} \cdot \pi}{b} \ [\text{s}^{-1}] \,, \tag{4}$$

where ω is the frequency of the EM emission, v_{el} represents the Rayleigh velocity, and "b" is the width of the crack. However, *Martinelli et al. (2020)* use the Rayleigh velocity, while in our calculation there was only seismic P wave velocity considered because of the material compression. According to the calculation, there were expected radio anomalies caused by the above-mentioned processes (piezo-electromagnetic phenomenon, triboelectricity etc.) on the slide surface in the frequency band from 15 kHz to 23 kHz.

3. Results

In the time records of electromagnetic field intensity in the VLF spectrum and seismic signals, there were observed significant similarities in the signals in the time 00:22:45 to 00:24:50.

The VLF spectrum, with a "custom" filter applied, has started at 6 kHz and has ended at 18 kHz, divided into 2 kHz segments. The seismic signal was filtered as well, primarily in the frequency range from 2 Hz to 10 Hz, as there was interest in local quakes. Global earthquakes are observable in the frequency range of 0.1 Hz $-$ 0.8 Hz or in the range of 0.7 Hz to 2 Hz for regional earthquakes.

The recorded anomaly in the VLF spectrum consists of two segments. The first was a peak at time 00:23:00, recorded in the VLF range from 11 kHz to 18 kHz, defined by a change in intensity of +3.7 dB. The range from 6 kHz to 10 kHz was not affected by this event. The same peak could be observed on the intensity scale of the seismic signal. Subsequently, after this first event, operationally termed the "initialization event", another longer event followed, characterized by an increase in the intensity of the VLF electromagnetic field by 6.8 dB with small fluctuations during the maximum duration (Fig. 5). In the seismic record, there was observed an identical signal at the same time with the same duration. The event was lasting for 50 seconds at its peak without the initial peak in both records.

Through mathematical correlation analysis of the entire record, there was obtained a correlation coefficient value $r = 0.84$, representing a relatively strong correlation between the VLF signal and the seismic signal
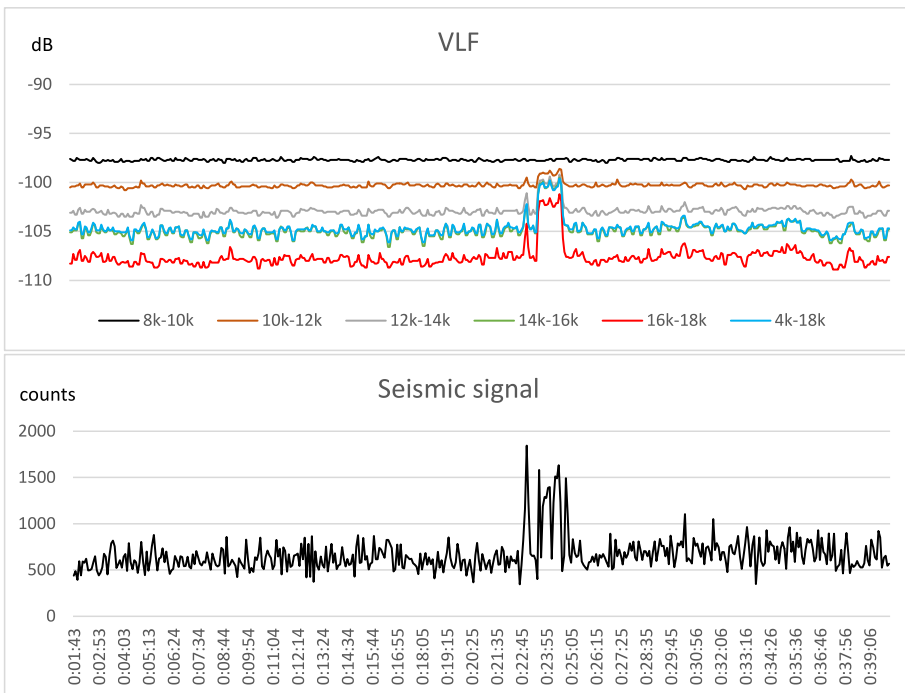

Fig. 5. Time course of changes in the VLF EM field and the time course of the seismic signal on May 16th, 2023, from 00:00:03 to 00:41:31, location Stoček.

during the event on nearby landslide bodies in the vicinity, either around
the active landslide between Kamenica and the Stoček site, with evident
terrain deformations during recorded period.

The highest correlation was captured in the VLF range of 16 kHz – 18 kHz
(Table 1). These radio emissions originating from the geological environ-
ment were precisely in the range that had been expected through phenomena
outlined in *Hoffman (2023)*.

Table 1. Results of mathematical correlation analysis of the entire time interval of VLF
divided into 2 kHz segments from 6 kHz to 18 kHz and the seismic signal.

Time shift (s)/ VLF (kHz)	6k–8k	8k–10k	10k–12k	12k–14k	14k–16k	16k–18k	4k–18k
−5	−0.031	0.011	0.670	0.758	0.735	0.783	0.751
0	−0.037	0.035	0.728	0.806	0.779	0.828	0.795
5	−0.042	0.056	0.751	0.824	0.796	0.840	0.811
10	−0.045	0.074	0.749	0.812	0.788	0.827	0.800
15	−0.035	0.066	0.716	0.772	0.755	0.793	0.765
20	−0.019	0.057	0.668	0.721	0.707	0.742	0.715
25	0.0073	0.054	0.611	0.661	0.649	0.682	0.657
30	0.0309	0.056	0.563	0.612	0.607	0.639	0.616
35	0.0503	0.053	0.537	0.590	0.586	0.617	0.595

The data in the seismic record are in 'counts', where 3.27508E9 counts
represent motion of 1 m.s^{-1}. Mentioned event on May 16th, 2023, was one
of the most significant ones that had been managed to be recorded.

The entire recording length was approximately 41.5 minutes and was cap-
tured from 00:00:03 to 00:41:31 (all recordings are from night-time hours).
In subsequent recordings, there wasn't such a high correlation coefficient
achieved. This was explained by the fact that there was a minimum of in-
put noise from the surroundings on that day, and the anomalies were truly
significant, contrasting sharply with the noise in both the VLF and seismic
signals.

Another record presented in this paper is from June 1st, 2023, from
04:00:03 to 04:46:36. Also this one was a night-time or early-morning record-
ing. There was an anomaly in this recording observed from 04:22:10 to
04:24:40, lasting approximately 2.5 minutes, composed of several shorter
vibrations.

The same count will be evaluated for the VLF recording. Like the previous event, the anomaly in the seismic record was characterized by an "initialization" peak. The highest correlation coefficient was in the frequency range of 18 kHz – 23 kHz, specifically $r = 0.66$, indicating a high correlation (Fig. 6, Table 2). The data in the graphs show a similarity in the shape of the seismic and VLF signal profiles.
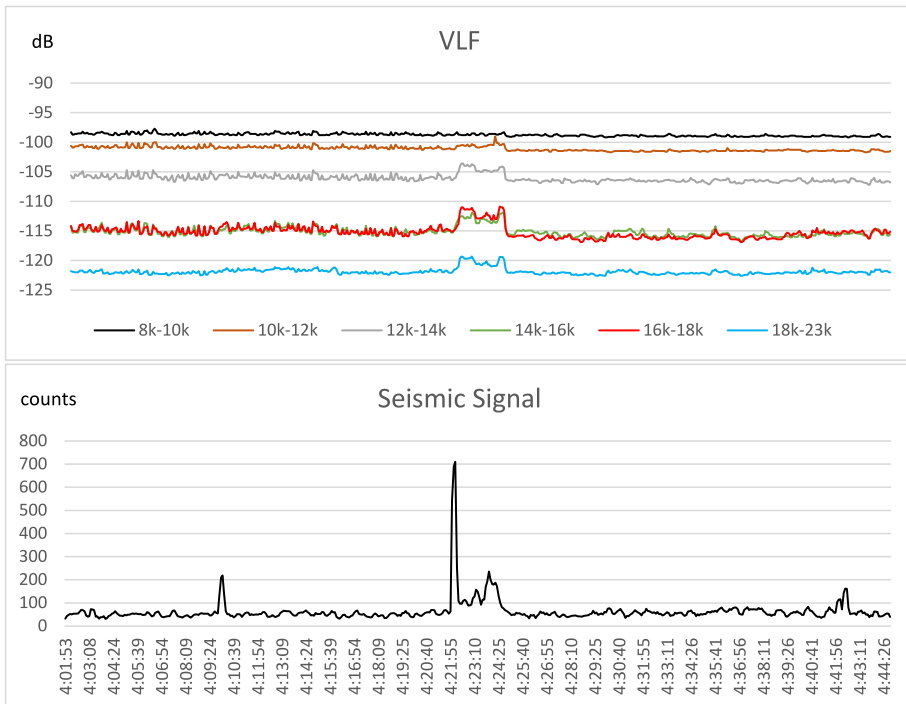

Fig. 6. Time course of changes in the VLF EM field and the time course of the seismic signal on June 1st, 2023, from 04:00:03 to 04:46:36, location Stoček 1 km from Kamenica.

They are almost identical, which likely indicates a common source, in our case, the geological environment – slide surfaces – a landslide composed of claystones and sandstones from the Beladice formation of the Panonian-Pontian age.

In the data tables, it is possible to observe a phenomenon of delay in the VLF signal ranging from 5 seconds on May 16th, 2023, to 15 seconds during the event on June 1st, 2023. The offset observed in the VLF signal, lasting

Table 2. Results of mathematical correlation analysis of the entire time interval of VLF divided into 2 kHz segments from 6 kHz to 18 kHz and the seismic signal.

Time shift (s)/ VLF (kHz)	6k–8k	8k–10k	10k–12k	12k–14k	14k–16k	16k–18k	18k–23k
−10.000	−0.021	0.042	0.179	0.294	0.359	0.333	0.375
−5.000	−0.026	0.049	0.213	0.354	0.407	0.386	0.444
0.000	−0.031	0.046	0.248	0.420	0.450	0.447	0.514
5.000	−0.044	0.024	0.270	0.476	0.475	0.500	0.578
10.000	−0.063	−0.005	0.272	0.509	0.484	0.543	0.629
15.000	−0.061	−0.010	0.274	0.534	0.487	0.574	0.663
20.000	−0.057	−0.008	0.276	0.537	0.484	0.577	0.660
25.000	−0.069	−0.015	0.255	0.518	0.470	0.563	0.646

up to 15 seconds in one scenario (typically ranging from 0 to 5 seconds in other cases), can be elucidated by the delayed occurrence of the VLF signal when a specific pressure threshold in the rock mass is exceeded.

In situations involving a delayed VLF signal, its generation occurs subsequent to the surpassing of a defined pressure threshold in the rock mass. In two other cases, there is a delayed seismic signal, ranging from 0 to a maximum of 5 seconds.

In this scenario, we can calculate the distance of the source based on the propagation speed of seismic waves in the geological substrate under our conditions, claystones and sandstones, seismic velocity ranging from $350 - 700$ m.s^{-1} up to 1500 m.s^{-1} (*Otepka et al., 1983; Tonnellier et al., 2013*). The landslide area is over 20 km long. Longer time delays of the seismic signal than 5 seconds were not measured in either case (there were several events throughout the year 2023, but there were two selected representative events with VLF delay), confirming that deformations most likely origination of the monitored area.

The consideration that the microseismic signal originated from a local source was confirmed by the fact that the frequency of the seismic signal is high, ranging from 5 Hz to 15 Hz (Fig. 7).

Microseismic tremors in a similar frequency range captured in landslide areas were also indicated in the work of *Martinelli et al. (2020)*. In Figure 7, there is an observation of nocturnal behavior of VLF (line graph overlaid on the seismic spectrogram) and the seismic component (spectrogram). In
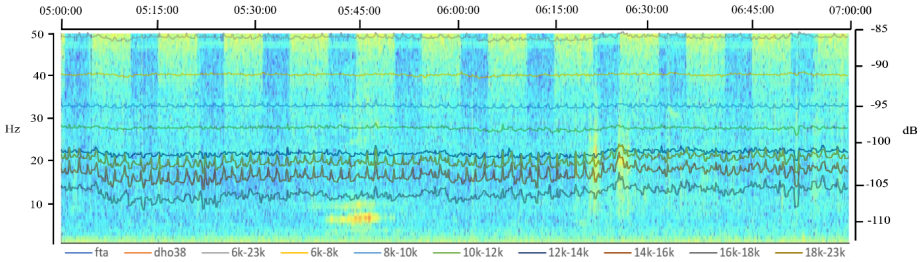
Fig. 7. Comparison of night activity (04:59:56 – 07:01:50 UTC) between the seismometer and VLF EM field on January 14, 2023, four days after rainfall exceeding 12 mm/24 hours; temperature 10 °C (y axis is amplitude of VLF and seismic signal, x axis is time in hour and second).

the graphical representation, anomalies are shown at 5:45 and 6:20 in both the seismic and VLF EM field change records. Regular anomalies in the seismic spectrogram are caused by an anthropogenic source, specifically a nearby water pump (a known signal that was filtered out from the correlation analysis).

Online in-situ comparison of VLF EM intensity and seismic event is on Figure 8. All known anthropogenic and natural radio anomalies, along with
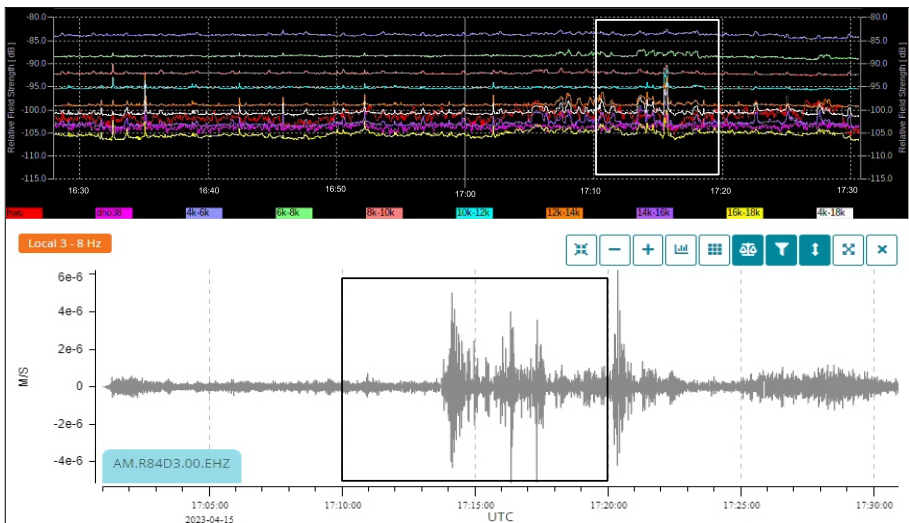

Fig. 8. Online comparison VLF EM intensity and seismic signal directly via web interface of seismometer on April 15, 2023.

their spectral shapes, had been already described in the work (*Hoffman, 2023*).

4. Discussion and conclusion

Using the equipment located in the landslide zone, it was possible to record micro-tremors and anomalies in the VLF radio spectrum. These radio anomalies temporally and morphologically corresponded to the seismic signal recorded in the landslide. There were several events where a certain correlation during VLF and seismic signals could be observed, but there were two representative ones selected with the highest correlation factor. Correlation values of 0.84 were obtained through mathematical correlation analysis of collected and filtered data. The lowest correlation coefficient for the analysed events was 0.36.

In total, 8 events were analysed in the time from March to June 2023. Pearson correlation coefficient "r" was used for correlation calculation. The frequencies, with expected anomalous signals originating from the rock environment were calculated from equation (3) and based on field observations (sizes of cracks, speed of seismic wave propagation in given geological conditions, etc.).

The seismic signal came from a local source, confirmed by the fact that the frequency of the seismic signal was high, ranging from 5 Hz to 15 Hz. During the mentioned time period of the observed events, deformations were observed in the form of block detachments and creeping deformations in the field. However, there is a belief of the captured signals, both seismic and VLF originated in the internal deformation of the landslide slope, meaning their source (slide surface of landslide), with a location at depths of 20 to 30 m.

Offset of the VLF signal, in one case with duration up to 15 seconds (for other events, it ranges from 0 to 5 seconds), can be explained by the delayed VLF signal occurring when a certain pressure threshold in the rock mass is exceeded. In cases of delayed VLF signal, this has been generated after surpassing a certain pressure threshold in the rock mass. Thus, the sliding slope is in motion, but the force acting on the rocks forming the fill of the landslide slope has not yet sufficient to create an EM impulse. This impulse was generated only after several seconds, ranging from 0 to 15 seconds.

In two cases, there is an assumption of delayed seismic signal because of passing through a discontinuity in the form of transverse tectonic faults that intersected the entire landslide area. Time delay of 15 seconds could be explained by considering the lowest velocity of seismic wave propagation (considered the most realistic velocity given the afore mentioned geological-tectonic conditions) through clay and sandstone at $350 - 700$ m.s^{-1} up to 1500 m.s^{-1} (*Otepka et al., 1983; Tonnellier et al., 2013*) and the source of this signal with a distance up to 10.5 km.

It is also necessary to consider aquifers, as well as the fact that the seismic wave velocity is lower in the landslide body, layers of clay and unconsolidated sand alternate than in compact rocks (sandstone, claystone). It's important to consider that EM emissions originating in the geological substrate could occur before, during, and after deformation in the landslide body, which may distort or even explain the offset between the VLF signal and the seismic signal.

Of course, we also verified whether the signal was not caused by electronic noise from the recording device or whether the receiving coils in the geophone and the loop antenna themselves were not influenced by external anthropogenic electromagnetic fields. If the coils were affected, the time of the anomalous signal of both the seismometer and the VLF receiver would be precisely identical (to the millisecond), but this did not occur in either case (the measurement is covered by time accuracy using a GPS, 1PPS signal and an NTP server (accuracy 10 ms). Also, the anomalous recording would not be visible in the infrasound component (a future publication), which is recorded by a different principle than the geophone and VLF receiver.

References

Adler P. M., 2001: Macroscopic electroosmotic coupling coefficient in random porous media. Math. Geol., **33**, 1, 63–93, `doi: 10.1023/A:1007562326674`.

Amitrano D., Gaffet S., Malet J.-P., Maquaire O., 2007: Understanding mudslides through microseismic monitoring: the Super-Sauze (SouthEast French Alps) case study. Bull. Soc. Géol. Fr., **178**, 2, 149–157, `doi: 10.2113/gssgfbull.178.2.149`.

Arattano M., 1999: On the use of seismic detectors as monitoring and warning systems for debris flows, Nat. Hazards, **20**, 2-3, 197–213, doi: 10.1023/A:1008061916445.

Blaha P., Duras R., 2004: Natural high frequency electromagnetic field on the Karolinka landslide. EGRSE, Int. J. Explor. Geophys. Remote Sens. Environ., **XI**, 1-2, 30–32.

Buescher W., 2020: SpectrumLab, Manual. Accessed at: https://www.qsl.net/dl4yhf/speclab/SpecLab_Manual.pdf.

Eccles D., Sammonds P. R., Clint O. C., 2005: Laboratory studies of electrical potential during rock failure. Int. J. Rock Mech. Min. Sci., **42**, 7-8, 933–949, doi: 10.1016/j.ijrmms.2005.05.018.

Fabo P., Gajdoš V., Blaha P., 2004: The sources of 14 kHz EM fields observed at geo-electrical measurements. EGRSE, Int. J. Explor. Geophys. Remote Sens. Environ., **XI**, 1-2.

Fiorucci M., Martino S., Della Seta M., Lenti L., Mancini A., 2022: Seismic response of landslides to natural and man-induced ground vibrations: Evidence from the Petacciato coastal slope (central Italy). Eng. Geol., **309**, 2022, 106826, doi: 10.1016/j.enggeo.2022.106826.

Gershenzon N., Bambakidis G., 2001: Modeling of seismo-electromagnetic phenomena. Russ. J. Earth Sci., **3**, 4, 247–275.

Hanson D. R., Rowell G. A., 1980: Electromagnetic radiation from rock failure. Report of Investigation no. 8594, Colorado School of Mines, Colorado, USA.

Hayakawa M., 2015: Earthquake prediction with radio techniques. John Wiley & Sons, Singapore Pte. Ltd., ISBN: 9781118770160, p. 125.

Heister K., Kleingeld P. J., Keijzer T. J. S., Loch J. P. G., 2005: A new laboratory set-up for measurement of electrical, hydraulic and osmotic fluxes in clays. Eng. Geol., **77**, 3-4, 295–303, doi: 10.1016/j.enggeo.2004.07.020.

Hoffman M., 2022: On potential use of natural electromagnetic emissions in ELF, VLF and HF radio bands at active landslide areas: Preliminary results from Vinohrady nad Vahom site (Slovakia). Contrib. Geophys. Geod., **52**, 1, 113–125, doi: 10.31577/congeo.2022.52.1.5.

Hoffman M., 2023: Preliminary catalogue of natural and anthropogenic VLF radio spectral patterns Contrib. Geophys. Geod., **53**, 2, 151–166, doi: 10.31577/congeo.2023.53.2.4.

Jaroševič A., Kundracík A., 2004: Measurement of the natural high-frequency magnetic field (PEE) in the boreholes using FJV99 selective picoteslameter. EGRSE, Int. J. Explor. Geophys. Remote Sens. Environ., **XI**, 1-2, 8–12.

Kharkhalis N. R., 1995: Manifestation of natural electromagnetic pulse emission on landslide slopes. Geophys. J., **14**, 4, 437–443.

Koktavý P., Šikula J., 2004: Physical model of electromagnetic emission in solids. In: Proc. 26th Eur. Conf. Acous. Emission Testing, EWGAE 2004, Berlin, Germany.

Krumbholz M., 2010: Electromagnetic radiation as a tool to determine actual crustal stresses – applications and limitations. PhD. Thesis, Mathematisch-Naturwissenschaftliche Fakultät, Georg-August-Universität, Göttingen.

Lin C. H., Jan J. C., Pu H. C., Tu Y., Chen C. C., Wu Y. M., 2015: Landslide seismic magnitude. Earth Planet. Sci. Lett., **429**, 122–127, doi: 10.1016/j.epsl.2015.07.068.

Maniak K., 2015: Measuring Electromagnetic Emissions from Active Landslides. J. Telecommun. Inf. Technol., **2015**, 2, 44–51.

Maniak K., Mydlikowski R., 2023: Apparatus for the Measurement of Electromagnetic Activity of Landslides. Adv. Sci. Technol. Res. J., **17**, 3, 184–195, doi: 10.12913/22 998624/166202.

Martinelli G., Plescia P., Tempesta E., 2020: Electromagnetic Emissions from Quartz Subjected to Shear Stress: Spectral Signatures and Geophysical Implications. Geosciences, **10**, 4, 140, doi: 10.3390/geosciences10040140.

Mastow R. Sz., Jaworowicz W. L., Gold R. M., 1989a: Electromagnetic activity during rock fracture (Elektromagnitnaja aktiwnost pri reologiczeskich ispitaniach gornych porod). Engineering Geology (Inzenernaja Geologia), 2/1989, 121–124 (in Russian).

Mastow R. Sz., Rudko G. I., Sałomatin W. N., 1989b: Electromagnetic activity in clay landslides s (Elektromagnitnaja aktiwnost pri razwitii opolzniei glinistych otłożeniach). Engineering Geology (Inzenernaja Geologia), 6/1989, 119–122 (in Russian).

Otepka J., Menzelová O., Bohyník J., Mesko M., Čubríková E., Roháčiková A, Škriepková Ľ., Novotný P., Čellár S., Abelovič J., Čerňanský J., Kúdela P., Bláha P., 1983: Hlohovec – Sereď, prieskum a sanácia zosuvov (Hlohovec – Sereď, survey and repair of landslides). Orientačný inžinierskogeologický prieskum, správa IGHP Bratislava (in Slovak).

Pearson K., 1907: On further methods of determining correlation. Drapers' Company Research Memoirs Biometric Series IV, Dulau and Company 39 p.

Rabinovitch A., Frid V., Bahat D., Goldbaum J., 2000: Decay mechanism of fracture induced electromagnetic pulses, J. Appl. Phys., **93**, 9, 5085–5090, doi: 10.1063/1. 1562752.

Raspberry manual: Raspberry Boom and Shake – seismometer with infrasonic detector. Accessed at: https://manual.raspberryshake.org/.

Raspberry data: Raspberry Boom and Shake – seismic data to download. Accessed at: https://data.raspberryshake.org/fdsnws/dataselect/1/builder.

Reppert P. M., Morgan F. D., Lesmes D. P., Jouniax L., 2001: Frequency dependent streaming potentials. J. Colloid Interface Sci., **234**, 1, 194–203, doi: 10.1006/jcis. 2000.7294.

Schumann K., Stipp M., Behrmann J. H., Klaeschen D., Schulte-Kortnack D., 2014: P and S wave velocity measurements of water-rich sediments from the Nankai Trough, Japan. J. Geophys. Res. Solid Earth, **119**, 2, 787–805, doi: 10.1002/2013JB010290.

Takeuchi A., Nagahama H., 2006: Electric dipoles perpendicular to a stick-slip plane. Phys. Earth Planet. Inter., **155**, 3-4, 208–218, doi: 10.1016/j.pepi.2005.12.010.

Tonnellier A., Helmstetter A., Malet J.-P., Schmittbuhl J., Corsini A., Joswig M., 2013: Seismic monitoring of soft-rock landslides: the Super-Sauze and Valoria case studies. Geophys. J. Int., **193**, 3, 1515–1536, doi: 10.1093/gji/ggt039.

Vybíral V., 2002: The PEE method helps assess slope stability. Laboratory and Field Observations in Seismology and Engineering Geophysics, Institute of Geonics of the AS CR, Ostrava-Poruba, Czech Republic.

Yamada M., Matsushi Y., Chigira M., Mori J., 2012: Seismic recordings of landslides caused by Typhoon Talas (2011), Japan. Geophys. Res. Lett., **39**, 13, L13301, `doi: 10.1029/2012GL052174.`